Journal of Hydrology 558 (2018) 366–379

Contents lists available at ScienceDirect

Journal of Hydrology

journal homepage: www.elsevier.com/locate/jhydrol

Research papers

Hillslope response to sprinkling and natural rainfall using velocity and celerity estimates in a slate-bedrock catchment

Anna Scaini [a,b,*], Christophe Hissler [a], Fabrizio Fenicia [c], Jérôme Juilleret [a], Jean François Iffly [a], Laurent Pfister [a], Keith Beven [b]

[a] Luxembourg Institute of Science and Technology (LIST), Environmental Research and Innovation Department (ERIN), Catchment and Eco-Hydrology Research Group (CAT), L-4422 Belvaux, Luxembourg
[b] Lancaster Environment Centre, Lancaster University, Lancaster LA1 4YQ, UK
[c] Eawag, Swiss Federal Institute of Aquatic Science and Technology, 8600 Dübendorf, Switzerland

ARTICLE INFO

Article history:
Received 28 February 2017
Received in revised form 31 July 2017
Accepted 3 December 2017
Available online 06 December 2017
This manuscript was handled by L. Charlet, Editor-in-Chief, with the assistance of Federico Maggi, Associate Editor

Keywords:
Velocity
Celerity
Fractured bedrock
Tracer experiments
Bedrock cleavage

ABSTRACT

Subsurface flow is often recognized as a dominant runoff generation process. However, observing subsurface properties, and understanding how they control flow pathways, remains challenging. This paper investigates how surface slope and bedrock cleavage control subsurface flow pathways in a slate bedrock headwater catchment in Luxembourg, characterised by a double-peak streamflow response. We use a range of experimental techniques, including field observations of soil and bedrock characteristics, and a sprinkling experiment at a site located 40 m upslope from the stream channel. The sprinkling experiment uses Br^- as a tracer, which is measured at a well downslope from the plot and at various locations along the stream, together with well and stream hydrometric responses. The sprinkling experiment is used to estimate velocities and celerities, which in turn are used to infer flow pathways. Our results indicate that the single or first peak of double-peak events is rainfall-driven (controlled by rainfall) while the second peak is storage-driven (controlled by storage). The comparison between velocity and celerity estimates suggests a fast flowpath component connecting the hillslope to the stream, but velocity information was too scarce to fully support such a hypothesis. In addition, different estimates of celerities suggest a seasonal influence of both rainfall intensity rate and residual water storage on the celerity responses at the hillslope scale. At the catchment outlet, the estimated of the total mass of Br^- recovered in the stream was about 2.5% of the application. Further downstream, the estimate mass of Br^- was about 4.0% of the application. This demonstrates that flowpaths do not appear to align with the slope gradient. In contrast, they appear to follow the strike of the bedrock cleavage. Our results have expanded our understanding of the importance of the subsurface, in particular the underlying bedrock systems, and the importance of cleavage orientation, as well as topography, in controlling subsurface flow direction in this catchment.

1. Introduction

Subsurface flow can be a dominant mechanism in runoff generation and has been widely investigated (Dunne, 1978; Hewlett and Hibbert, 1967; Whipkey, 1965). Subsurface flow takes place both in the soil matrix (Beven, 2010; Gilman and Newson, 1980; Jones and Crane, 1984; Uchida et al., 2005), and in soil cracks located between the soil and an impeding layer, earthworm burrows, root channels or other forms of macropores which enable the movement of water (Beven and Germann, 1982; Bryan and Jones, 1997; Chappell, 2010; Jackson, 1992).

Runoff generation processes are typically studied at the hillslope scale (Dunne, 1978). Notwithstanding recent advances in measuring techniques, measuring subsurface flow, as well as the subsurface properties that control subsurface flow, remains impracticable at other than the scale of small cores (Gabrielli et al., 2012; Hale and McDonnell, 2016; Wienhöfer and Zehe, 2014).

Besides the soil properties, the bedrock structure can have a strong influence on subsurface runoff. Although hard bedrock is often considered impermeable (Tromp-van Meerveld et al., 2007; Weyman, 1973; Wrede et al., 2015), this assumption is often "hopeful rather than realistic" (Beven, 2006). Fractured bedrocks are very common in Europe (Lorz et al., 2011), and flow through bedrock can be substantial (Padilla et al., 2015; Tromp-van Meerveld et al., 2007). Hale et al. (2016) identified subsurface

* Corresponding author at: Lancaster Environment Centre, Lancaster University, Lancaster LA1 4YQ, UK.
E-mail address: a.scaini@lancaster.ac.uk (A. Scaini).

https://doi.org/10.1016/j.jhydrol.2017.12.011
0022-1694/

permeability structures as the main control on water storage and release. Permeable bedrocks pose additional challenges regarding the identification of subsurface water release to the stream (Cook et al., 2003; Sklash and Farvolden, 1979). The geometry of fractures, which depends on the parent lithology and history (Chappell et al., 2007; Onda et al., 2001), can cause extreme spatial variability of hydraulic conductivity and groundwater flow rate (Cook et al., 1996, 2003).

In order to understand how fractured bedrocks control hydrologic response it is necessary to describe each of the involved subsurface flowpaths and storage structures (Banks et al., 2009; Hale et al., 2016). This approach, however is impractical, particularly for large areas. Therefore, more commonly, subsurface properties are inferred using other techniques, such as by using geochemical tracers (Harr, 1977; Sidle et al., 1995).

Tracer studies are employed to understand how quickly, in what concentration and from what sources water reaches the stream. Tracer input-output relationships are used to estimate the transit-time distributions of water in the catchment (Klaus et al., 2015; McGuire et al., 2007; Nyberg et al., 1999) and can be useful to characterise flowpaths (Trudgill et al., 1983; Wienhöfer and Zehe, 2014). Unfortunately, the interpretation of the tracer results is often biased by the spatial and temporal resolution and analytical protocols of tracer collection (Abbott et al., 2016; Weihermüller et al., 2007).

Tracer data can also be used to estimate velocities and celerities, which can aid the interpretation of subsurface flow pathways. In particular, differences between velocities and celerities are thought to explain the rapid runoff of stored water during rainfall events (McDonnell and Beven, 2014). However, few studies to date have quantified in-situ velocities and celerities. Novel model frameworks consider both celerity distributions, which manifest themselves in the hydrograph, and velocity distributions, manifested in tracer responses (Birkel and Soulsby, 2015; Davies et al., 2011; Laine-Kaulio et al., 2014; Scudeler et al., 2016; Soulsby et al., 2015). In a framework based on velocity/celerity analysis, the hydrograph and flow path velocity characteristics are integrated. While average celerity and average velocity can be estimated at catchment scales (Rasmussen et al., 2000), there have been very few studies that have attempted to study the characteristics of both celerities and velocities at field scale (Scaini et al., 2017).

Our work is undertaken in the Weierbach experimental catchment in Luxembourg, a site underlain by Devonian slate (Juilleret et al., 2011; Moragues Quiroga et al., 2017) characterised by double-peak runoff responses (Martínez-Carreras et al., 2016). We complement previous work (Scaini et al., 2017) which was based on the interpretation of estimates of maximum velocities and flow celerities during vertical infiltration, and showed that, at the plot scale, the flow direction in the soil profile is predominantly vertical, until the relatively impermeable boundary of the bedrock system is encountered. The impermeable layer is located at about 2–3 m below the surface (Scaini et al., 2017). The conditions required for the onset of lateral subsurface flow at the hillslope scale have not been previously investigated and are the focus of this complementary work.

Our objective is to quantify celerities and velocities in the path between the hillslope plot and the stream, by analysing artificial sprinkling experiments and stream chemistry. Specific research questions include:

(i) How are groundwater and streamflow dynamics related to rainfall inputs?
(ii) How do bedrock structural properties, particularly cleavage orientation, influence tracer transport from plot to stream?
(iii) How does tracer transport relate to estimates of celerities?

The manuscript is structured as follows: Section 2 presents the research site, followed by Section 3 where the equipment used is presented, and Section 4, describing the sprinkling experiments and the analysis applied. Section 5 describes results on hydrometric response to rainfall and sprinkling, tracer detection, and velocity and celerity estimates. Section 6 discusses each of these research questions. The paper concludes by summarizing the key findings of the study in relation to each of the research questions.

2. Description of the experimental field site

The Weierbach, an experimental site located in the North-West of Luxembourg, is a forested catchment underlain by Devonian slate. Altitudes range from 465 to 512 m a.s.l. Average annual rainfall is 812 m/a (2007–2016) and annual runoff ratios are around 0.55 (2005–2008) (Martínez-Carreras et al., 2016).

Geologically, the catchment soils are developed on Pleistocene Periglacial Slope Deposits overlying *in situ* compact and slightly weathered slate bedrock also called Saprock (Eggleton, 2001; Juilleret et al., 2011; Martínez-Carreras et al., 2016). The whole regolith classification is Dystric Cambisol (Ruptic, Endoskeletic, Siltic, Protospodic) according to the WRB reference (WRB, 2015) overlying a Regolithic Saprock (Vertifractic, Rootic) [Slatic] (Juilleret et al., 2016). The 64^2 plot used for the sprinkling experiments is located 40 m uphill from the stream, on the left bank (Fig. 1). The slope is steep (average of 10°) and perpendicular to the stream.

Rock cleavage or foliation is a property of rocks, referring to layering along approximately parallel surfaces (Singhal and Gupta, 2010). The cleavage planes lead to preferential cracks within the rock. Depending on the extent of connectedness and orientation, cracks can have a variable impact on water movement. At the hillslope site, a geological compass and clinometer measurement of the strike and dip of the cleavage plans showed on average 70 N degrees and a vertical dipping, in other words diagonally with respect to the surface slope (a sketch of its orientation is shown in Fig. 1b).

Previous work assumed that significant lateral (parallel to the surface topography) subsurface flow would occur in the fractured bedrock (or Saprock) or in the stony basal layer of the periglacial cover beds (Juilleret et al., 2016; Wrede et al., 2015). Our previous analysis, however, showed that the significance of lateral flow in the near-surface soil profile at the site is very low (Scaini et al., 2017). Thus subsurface hillslope contributions to streamflow should are expected only below 2–3 m in the fractured slate bedrock. This zone, however, is characterised by low porosity and resistivity, which complicates the detection of lateral flow using geophysical methods. Here we attempt to examine the hillslope to channel flow pathways by characterising the release of water from the hillslope, monitoring the outflow to the stream using tracers.

3. Materials

Considering the hillslope as a system, we present the equipment used to generate or measure (i) input of water and tracers; (ii) internal states, including water content and concentrations; (iii) output of water and tracers in the stream.

3.1. Input

Natural precipitation was recorded by a tipping bucket rain gauge (Campbell Scientific Ltd., model 52203) located 3.5 km from the experimental catchment, at the Roodt automatic weather station. The high density of vegetation hindered measurements of natural precipitation closer to the experimental plot.

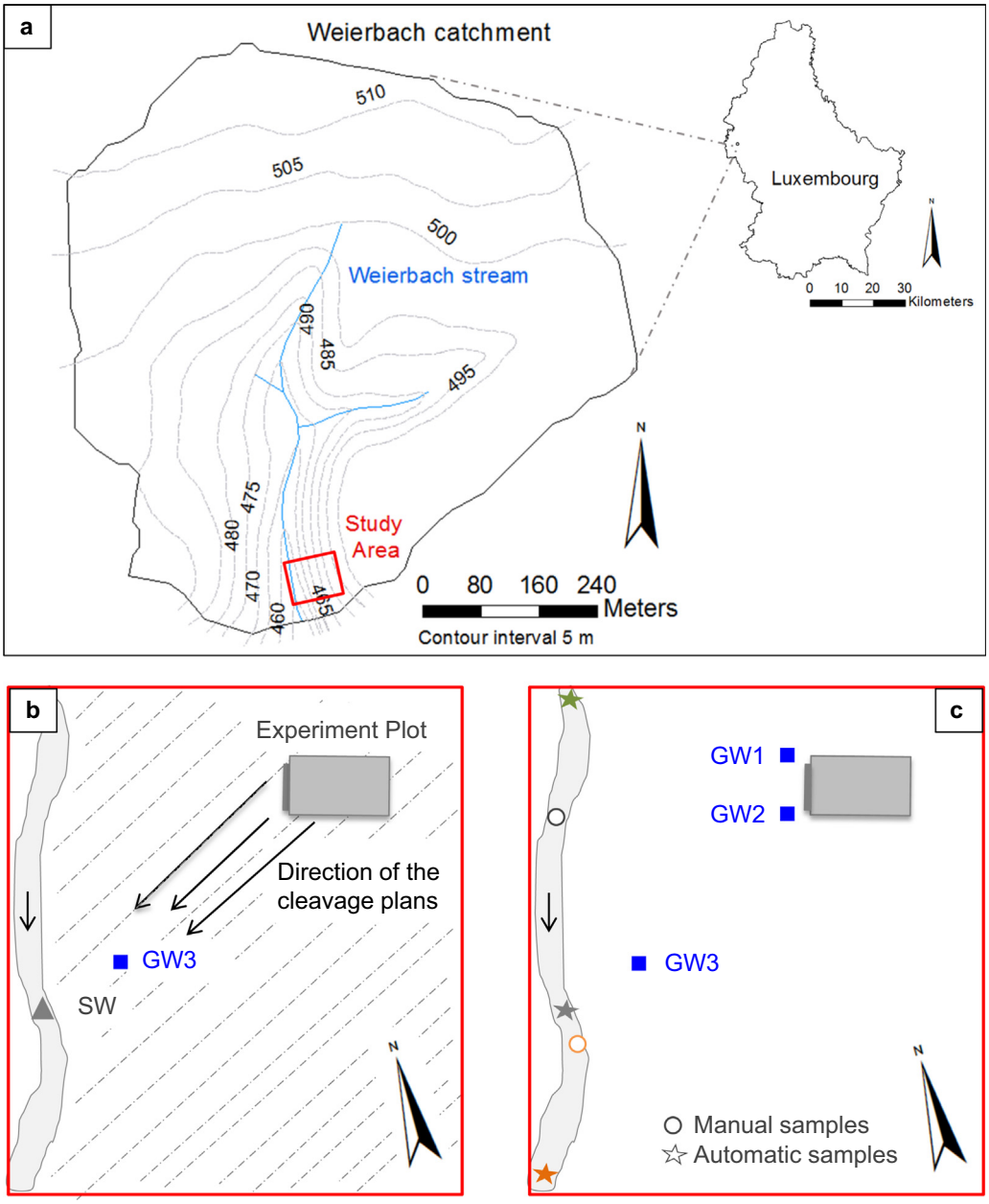

Fig. 1. (a) Location of the Weierbach catchment, in Luxembourg. The enlarged red box shows the location of the chosen hillslope within the Weierbach catchment. (b) The box shows the plot used for the sprinkling experiments, the location of the well GW3 (indicated by a blue square), and the stream gauge, SW (indicated by a grey triangle). (c) Sketch of the hillslope with the automatic (stars) and manual (circles) sampling points used during Experiment 2 to monitor the chemical composition of the stream water response to sprinkling. The location of the 2 wells GW1 and GW2 are also shown. (For interpretation of the references to color in this figure legend, the reader is referred to the web version of this article.)

3.2. Internal states

In order to detect lateral flow beneath the collection troughs, two groundwater wells, of 2-in diameter, were installed at the base of the plot. Drilling was performed from the surface of the forest road, on the two sides of the roof covering the base of the plot. The two wells were drilled to 2 (GW1) and 2.4 m (GW2) depth and equipped with pressure sensors for measurement of conductivity, temperature and water level (Hydromet OTT CTD, Fig. 1c). Additionally, a 3-in diameter groundwater well (GW3), located 12 m from the stream (Fig. 1b), was monitored for water table depth fluctuations, electric conductivity (EC) and temperature (using another OTT CTD sensor). The well GW3 was drilled in 2009 and was sited to follow the cleavage strike (Fig. 1b). The chemical composition of the well water was analysed with grab samples collected at variable time steps during the experiments. To characterise the evolution of the concentrations of the well outside the artificial experiments, bi-weekly samples were taken during a period of 2 years.

Finally, a 2-in groundwater well located on the plateau uphill of the study plot (GW4) was monitored for water table depth fluctuations, electric conductivity (EC) and temperature starting from September 2014 using a multi-probe TD-Diver (Schlumberger Water Services). As the monitoring was not permanent during the studied period, this well was used mostly as a reference for overall water table fluctuations.

3.3. Outputs

Stream water level at the outlet (SW) was measured using a pressure transducer (ISCO 4120 Flow Logger) in combination with a V-notch weir. EC at the outlet was also continuously monitored using a conductivity probe (WTW 3310). The chemical composition of the stream water at SW was monitored during a period of 2 years using manual bi-weekly samples. Additionally, a high resolution stream sampling set-up was undertaken during the sprinkling experiments. The stream was sampled at 3 different locations: (i) at SW (the outlet) (ii) 30 m upstream (upstream respect to the study hillslope) and (iii) 15 m downstream using automatic water samplers (ISCO 6712, Fig. 1c). Manual samples were also manually collected at 2 intermediate locations (Fig. 1c).

4. Methods

This section describes the measurements performed during the sprinkling experiments (Section 4.1) and the analyses of the measured data collected during the experiments (Section 4.2).

4.1. Sprinkling experiments

Artificial irrigation experiments were carried out between March 31st and April 10th 2014 (Experiment 1) and had the aim to explore plot-scale generation of shallow lateral flow, described in Scaini et al. (2017). Experiment 1 raised the need for additional monitoring of the stream to help understand the subsurface flow pathways. Experiment 2 was therefore performed using different tracers between March 11th and 16th 2015. For a full description of the experiments and analysis of flows in the near-surface soil, see Scaini et al. (2017).

4.1.1. Plot scale monitoring: Experiment 1

During Experiment 1, solutions containing different concentrations of NaCl and KBr were used to sprinkle the area. The sampling protocol was mostly carried out at the plot scale to characterise plot response. Given some shortcomings in the experimental design (absence of shallow lateral flow, limited information on deeper storage, need of including stream sampling to study the release of water from the hillslope), described in Scaini et al. (2017), we refined the methodology and experimental design in a second experiment.

4.1.2. Stream intensive sampling: Experiment 2

During Experiment 2, solutions of water and NaCl were applied, and additional data were used to monitor hillslope response. The stream was sampled at high frequency at 3 locations (Fig. 1c, stars) using ISCO automatic samplers (Section 3.3) programmed at 30 min time step during the experiment, and progressively longer time steps for a period of 3 weeks after the experiment (from 1 h to 6 h time step). Manual samples were taken at 2 locations at hourly time step during the experiment (Fig. 1c, circles).

4.2. Analyses of measured data

4.2.1. Hydrometric monitoring

During the experiments, the water table depth fluctuations, EC and temperature were recorded at 15-min intervals in GW3. In order to capture lower lateral flow, the two wells at the bottom of the plot, GW1 and GW2 in Fig. 1c, recorded water table height, temperature and EC at variable time step (up to 5 s time step during the experiments). Runoff and EC at the outlet (grey star, Fig. 1b) were continuously recorded at 15-min intervals.

4.2.2. Natural rainfall events analysis

A series of natural rainfall events were considered for the analysis. The selection criteria focused on rainfall events of a total of at least 15 mm, to analyse event magnitudes as much as possible similar to the sprinkling. Each event was considered separately when the time elapsed from the previous event was at least 3 h, as during the sprinkling experiments each day's irrigation was carried out non-stop or stopped for a period between 1 and 3 h. Rainfall intensity, catchment wetness (in terms of Antecedent Precipitation Index, API, calculated for 30 and 7 days prior to the rainfall event), and the timing of stream and groundwater response were calculated for each rainfall event. Cross-correlation was used to calculate the time-lag for which the correlation between rainfall and stream discharge was maximum. In the same way, the time-lag corresponding to the maximum correlation between rainfall and water table depth was also computed (in this case, maximum inverse correlation).

Double peaks in the hydrograph were observed from late autumn to early spring when soil moisture values are higher. There were also a few cases where summer double peak events occurred linked to large precipitation events (Martínez-Carreras et al., 2016). Cross-correlation was also computed for the double peak events. The results of cross-correlations were used to check for differences between single and double peak discharge and groundwater response timings.

4.2.3. Tracer monitoring

The arrival time of the tracers to each sampling point was determined by comparison with the background values. Tracers dissolved in the input water were used to track the water knowing precisely its input times and chemical composition.

All collected water samples were filtered using Acrodisc syringe 0.45 μm filters (Pall Corporation) in order to be analysed for chloride (Cl^-) and bromide (Br^-) concentrations using ionic chromatography (Dionex ICS-5000). The detection limit of the analyses was 0.01 mg L^{-1} for Cl^- and 0.02–0.01 mg L^{-1} for Br^-.

Background anions and cations in the stream and groundwater were measured over a three year long bi-weekly sampling campaign, between 2011 and 2013. The average value of the background Cl^- concentration in the input water was 3.33 ± 2.45 mg L^{-1}. No detectable Br^- concentrations were found in the background samples. The average EC value in the stream water was 45 ± 10 μS cm^{-1}. Cl^- detected in the well over the 3-years bi-weekly campaign were equal to 5.15 ± 0.42 mg L^{-1}, while EC had mean value of 107 ± 6 μS cm^{-1}. A linear regression model to estimate Cl^- from EC was fitted to such data (Chang et al., 1983; Siosemarde et al., 2010).

Br^- concentrations during the high frequency sampling stream campaign (Experiment 2, Section 4.1.2) were used to calculate the mass of Br^- leaving the system. This was performed by (i) interpolating the missing concentration data to hourly time-step; (ii) multiplying Br^- concentrations to discharge (available at hourly time step) to obtain the load; (iii) summing up all the values to obtain the total mass of Br^-.

4.2.4. Velocity estimates

Given the importance of both celerity and velocity in storage-discharge responses (McDonnell and Beven, 2014), estimates of both quantities were derived using a data-based approach. For both velocities and celerities, a time difference and distance are required.

A velocity distribution summarizes the range of velocities of water particles within the subsurface. Wider distributions are indicative of larger heterogeneities and variability of flow pathways, whereas narrower distributions are representative of more homogeneous conditions (Davies and Beven, 2012). Maximum

velocity can be derived as the first detection of a tracer at a measurement point and represents the fastest flow pathway (McDonnell and Beven, 2014). Mean velocity provides information on propagation, storage and remobilisation of tracers.

Maximum and mean velocity determined from the tracer data and the information on the lengths and times used to compute each velocity are shown in Table 1a. The arrival times of Br^- and EC (used as a proxy for salt tracer) to well and stream, were used to estimate information on velocities. For the time information, each velocity was computed using tracer application as a starting point.

At the well GW3, the maximum velocity was computed by dividing the distance between the plot and the well by the time at which a start of EC rise (corresponding to the time at which the tracer plume reached the well) occurred ($v_{max,w}$) (Table 1a). The well EC peak provided time information regarding the arrival of the maximum concentration of the plume, an approximation of the mean velocity, $\bar{v}_w$. In the same way, the plot-stream downslope distance was divided by the time between start of tracer application and start of the EC rise in the stream, to compute the maximum velocity ($v_{max,s}$). The plot-stream downslope distance was divided by the timing of the stream EC peak to estimate the mean velocity, $\bar{v}_s$.

4.2.5. Celerity estimates

Celerity is defined with respect to the speed with which a perturbation to the flow propagates through the flow domain (McDonnell and Beven, 2014). Celerity responses depend on the nature of the perturbation and the antecedent wetness, which in our case is determined by the artificial and natural rainfall events. Defining a consistent framework to calculate the spatial propagation of a perturbation is critical to be able to look at the celerity estimates.

For the purposes of analysis we need to provide working definitions of celerities that can be calculated from the data. For the water table, we can assume that the first response following rainfall will be a good indication of first wetting celerity in the unsaturated zone (classically as a wetting front shock, Beven, 1981), but here more likely as a result of preferential flow. In the case of the stream, the initial rise will be a combination of the initial response in the riparian area and routing through the channel network. We can also define celerities based on the time to peak of the water table and hydrograph. For the water table response, this will represent an average for the unsaturated zone and saturated zone response upstream of the well. For the discharge, it represents and integral of the hillslope and channel network responses, including likely fast pathways through the bedrock fractures of hillslopes, as recent research suggested (Jackisch et al., 2016; Martínez-Carreras et al., 2016; Wrede et al., 2015). Thus we calculate the following celerity indices, as described in Fig. 2 and Table 1b, using the natural rainfall events described in Section 4.2.2:

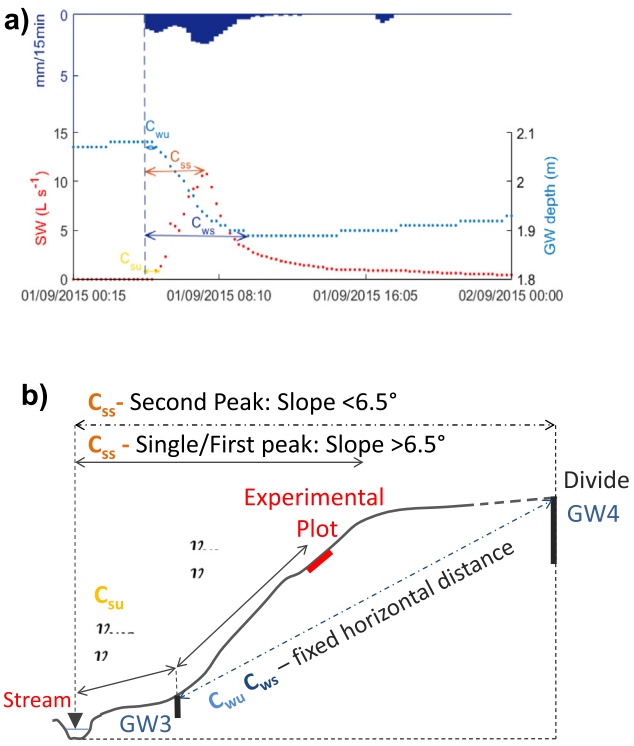

Fig. 2. Definition sketch for celerity calculations. (a) The figure shows time series of rainfall, SW discharge and GW depth for an event in 2015 (Event 19, Table 2). Celerity measurements refer to the time lag from the start of rainfall to the start of water table response, here shown as GW3 depth (C_{wu}), start of discharge response (C_{su}), maximum value of GW3 depth (C_{ws}) and discharge peak (C_{ss}). (b) Spatial framework for the estimation of celerities and velocities. The symbols correspond to Table 1.

1. Initial event celerity, C_{su}, was estimated using the time frame between rainfall start and start of discharge rise at outlet;
2. Integral event hydrograph celerity (C_{ss}) was estimated, using the time frame between rainfall start and peak discharge at the outlet;
3. Initial hillslope celerity (C_{wu}) was estimated using the time frame between rainfall and start of water table response in GW3;
4. Integral hillslope celerity (C_{ws}) was estimated using the time frame between rainfall start and peak of water table response in GW3.

Table 1
Definition table for velocities and celerities used throughout the paper. the definitions make reference to Fig. 2.

a) Symbol	Type	Length	Time (from tracer injection)
$V_{max,ws}$	Maximum velocity	From GW3 to stream	Start EC rise in SW
$\overline{v_{ws}}$.	Mean velocity	From GW3 to stream	Peak EC in SW
$V_{max,w}$	Maximum velocity	From plot to GW3	Start EC rise in GW3
$\overline{v_w}$.	Mean velocity	From plot to GW3	Peak EC in GW3
b) Symbol	Type	Length	Time (from rainfall start)
C_{su}	Initial event celerity	Average riparian zone length	Start discharge rise
C_{ss}	Integral event hydrograph celerity	Average hillslope length (including divide in second peaks)	Peak discharge
C_{wu}	Initial hillslope celerity	Planar distance between well located on top (GW4) and on bottom (GW3) of the slope	Start water table rise in GW3
C_{ws}	Integral hillslope celerity	Planar distance between well located on top and on bottom of the slope	Water table peak in GW3

To define the relevant downslope distances, we used a 5 × 5 DEM. In the single or first peak events, the distance was defined as the mean downslope distance between the stream and the hillslope (slope > 6.5°). In the double-peak events, the mean downslope distance between the stream and the divide (slope < 6.5°) was used to include the plateau, as in the formulation of Martínez-Carreras et al. (2016) (C_{ss}, Fig. 2b). Mean hillslope lengths used for the stream celerity (C_s) were defined using the following procedure: (i) computing the Euclidean distance to the stream for each pixel of the DEM; (ii) computing and clustering the slopes of the Weierbach (>6.5° and <6.5°); (iii) computing the average downslope distance for all the pixels >6.5° (corresponding to the hillslope) and <6.5° (plateau).

In the case of the well response, the fixed planar distance between the 2 wells located respectively on the plateau (GW4) and at the bottom of the slope (GW3) was used to compute information of celerity (Fig. 2b). Such measure was divided by the start of water table rise (to compute C_{wu}) and time of peak (to compute C_{ws}), both calculated from the start of the rainfall event.

5. Results

5.1. Response to natural rainfall and to sprinkling

Table 2 summarizes the characteristics of 21 natural events (12 in 2014 and 9 in 2015) having cumulative rainfall higher than 15 mm (Section 4.2.2). In addition to the characteristics of each rainfall event, the maximum cross-correlations between rainfall and groundwater, and rainfall and discharge responses are given for each event.

The relationship between time series was analysed as a first check for relationships between variables. The average of the maximum correlation coefficients (R) between rainfall and discharge, as used to indicate the average lag time, was equal to 0.66. In all cases the corresponding time lag was below 1 h, showing a relatively homogeneous response of the discharge to rainfall in terms of timing (Table 2). In the case of Event 19, the maximum correlation occurred for the non-lagged discharge, showing that the response to rainfall was quicker than 15 min, one time step (Table 2). The maximum lag time between rainfall and water table response ranged between 0.5 and 12.5 h (Table 2), with maximum R between 0.10 and 0.70, showing a more complex timing response. In all the single peak cases, the start of the discharge rising limb and discharge peak always preceded the first rise of the water table. In the cases where a double peak occurred, the discharge peak followed the maximum rise of the water table (measured from GW3), with peaks lagged between 1 and 3 h.

Fig. 3 shows the discharge-storage relationship (Fig. 3a) as well as the EC-well relationship (Fig. 3b), with a few events of more than 15 mm rainfall highlighted by colours (events 1, 2, 3, 7, 10, 12, Table 2). The event of December 2014, highlighted in yellow in Fig. 3, generated the highest water table (reaching 1 m below

Table 2
Rainfall events with cumulative rainfall >15 mm and characteristics of the rainfall event: event number, date, total mm, duration in hours, maximum intensity in mm/15 min, maximum intensity in mm h^{-1}, API30 and API7. For each event, the maximum cross-correlation expressed in minutes of lag between rainfall and GW3 response and rainfall and SW discharge response are shown. Bold: double peak events. Coloured: events highlighted in Fig. 3. Brackets: maximum correlation occurred for first peak only. X: absence of correlation.

n.	Date dd/mm/yyyy	mm tot	duration rainfall (h)	max mm/15min	max mm/h	API30 mm	API7 mm	GW3 lag min	SW lag min
1	**06/01/2014-07/01/2014**	**20.2**	**7.5**	**1.6**	**3.8**	**89.4**	**19.6**	**60**	**15**
2	04/06/2014	18.9	13	3.3	5.0	62.9	0.1	60	30
3	11/06/2014	17.3	1.5	10.9	15.7	43.4	19	30	15
4	06/07/2014	16.2	3.5	5.4	9.9	47.6	12.6	180	60
5	08/07/2014	16	15	1.2	4.0	64.1	22.2	192	15
6	09/07/2014	21.7	12	1.4	4.1	80.1	38.2	240	60
7	24/07/2014	18.5	0.5	9.7	18.4	101.6	0.7	45	15
8	29/07/2014	17	1.75	7.1	8.3	108.3	24.4	90	30
9	08/08/2014-09/08/2014	23.7	5.25	6.1	8.6	109.8	22.9	270	30
10	10/08/2014	22.8	7.5	12.3	12.7	114.9	49.7	330	15
11	**11/12/2014**	**15.5**	**18**	**1.6**	**3.4**	**28.9**	**7.3**	**585**	**(15)**
12	**12/12/2014-13/12/2014**	**31.2**	**22.75**	**0.6**	**1.7**	**57**	**36.4**	**x**	**x**
13	**08/01/2015**	**31.7**	**21**	1.2	**6.0**	**84**	**5.3**	**(30)**	**(60)**
14	**15/01/2015**	**26.5**	**26**	0.9	**2.8**	**87.4**	**56.5**	**1920**	**1260**
15	14/02/2015	19.8	20.5	3.6	6.6	71.6	23.3	75	15
16	29/03/2015-30/03/2015	20.9	26.5	2.1	4.6	27.2	8.6	135	30
17	04/08/2015	18.7	7	10.6	14.0	35.5	0.6	750	60
18	27/08/2015-28/08/2015	21.7	24	1.1	2.9	50.4	7.7	705	45
19	01/09/2015	32.3	8.25	2.4	8.8	71.5	25.2	180	<15*
20	15/09/2015-16/09/2015	47.5	17.5	11.3	14.7	82.4	17.6	120	15
21	**19/11/2015-20/11/2015**	**29.6**	**36**	**0.5**	**4.3**	**38.5**	**36.8**	**x**	**x**

*The maximum correlation occurred for the non-lagged discharge.

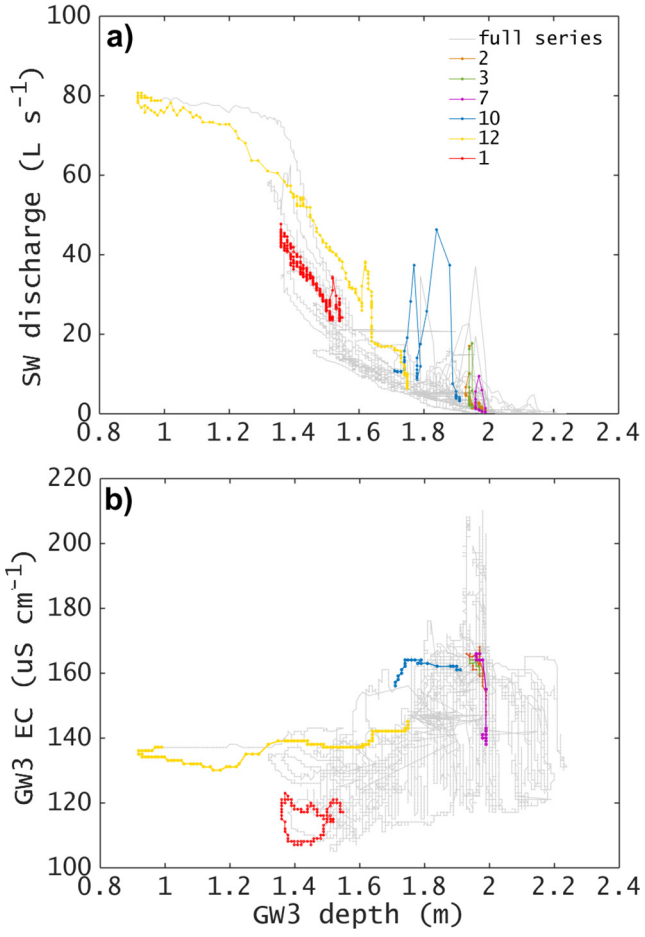

Fig. 3. (a) Scatterplot showing the relationship between SW discharge and depth to water table in GW3. (b) Scatterplot showing the relationship between depth to water table and corresponding value of EC, both measured in GW3. In both graphs the full series of 2014 and 2015 are shown in grey, while few events are indicated by colours (events 1,2,3,7,10,12 see Table 2).

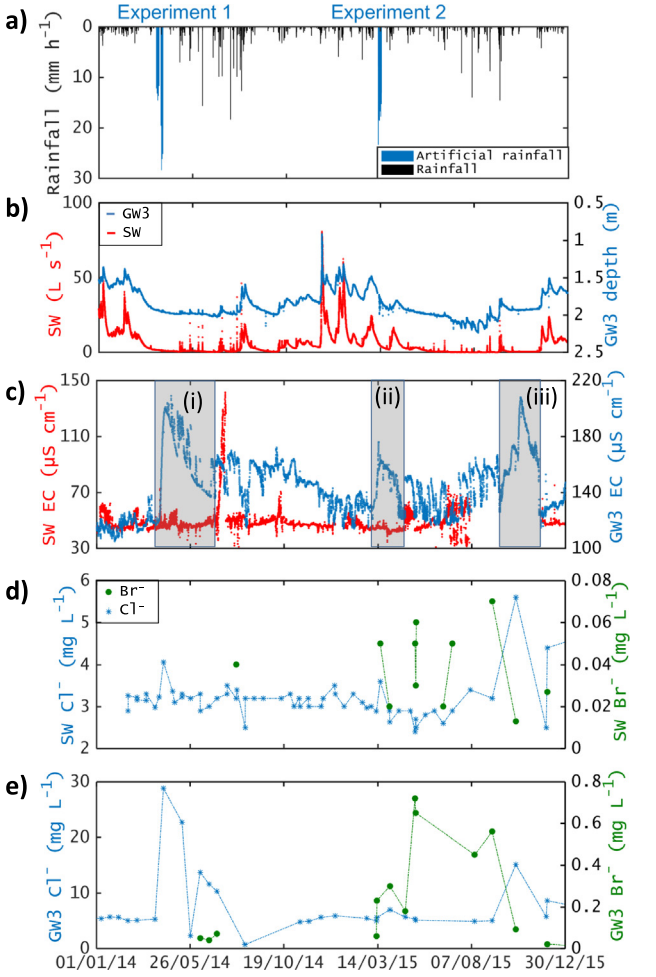

Fig. 4. (a) Time series of hourly natural (black) and sprinkled (light-blue) rainfall. (b) GW3 depth to the surface (light blue) and SW discharge at outlet (red). (c) Stream EC (red) and GW3 EC (light blue), both expressed as µS cm^{-1}. (d) Cl$^-$ (blue, left y axis) and Br$^-$ (green, right y axis) concentration measured at SW. (e) Cl$^-$ and Br$^-$ concentration in GW3. Br$^-$ concentrations below detection limit are not shown. Br$^-$ concentrations in SW are ten times lower than GW3 concentrations. (For interpretation of the references to color in this figure legend, the reader is referred to the web version of this article.)

soil surface) and discharge peak (up to 80 L s^{-1}). The relationship between water table depth and EC does not follow a clear pattern, even though we can see the peaks due to the tracing experiments, where despite the absence of response in the water table, the EC rose to the maximum values for the series (Fig. 3b).

The stream and GW3 were not affected by the experiments: both stream discharge and groundwater depth did not have a significant response during both Experiment 1 and Experiment 2.

Table 3 shows, for both Experiment 1 and 2, the minimum and maximum values of groundwater EC and depth to water table measured at GW3, and stream EC and discharge measured at SW. The maximum values of EC during the period following Experiment 1, resulting from the salt dissolved in the sprinkling water are given in brackets. Both experiments were conducted in low flow periods (discharge range 1–2 L s^{-1} in Experiment 1 and 4–7 L s^{-1} in Experiment 2).

Fig. 4 shows the time series of natural and sprinkled rainfall (a), GW3 depth to the surface and SW discharge (b), EC in SW (left y axis) and GW3 (right y axis) (c). Fig. 3d and e show respectively stream and GW3 Cl$^-$ and Br$^-$ concentrations, expressed as mg L^{-1}.

Following Experiment 1, detectable EC rises in GW3 were observed (Fig. 4c). Three distinct EC peaks were observed: (i) following Experiment 1; (ii) following Experiment 2; (iii) in late 2015 (indicated in Fig. 4c). The EC in GW3 started to rise on April

Table 3
The minimum and maximum values of sprinkled rainfall, EC and water table depth (measured in GW3), EC and discharge (measured at SW) are shown. The maximum EC values occurred after the first experiment – likely due to arrival of sprinkled salts – are shown in brackets.

		Rainfall mm h^{-1}	GW3 EC uS cm^{-1}	GW3 depth m	SW EC uS cm^{-1}	SW discharge L s^{-1}
Exp 1	Max	23.4	136 (201)	1.96	73 (145)	2.0
	Min	5.1	117	1.93	43	1.0
Exp 2	Max	28.4	176	1.89	47	7.0
	Min	5.1	136	1.73	44	4.0

09th and peaked on April 18th, 2014 with 201 μS cm^{-1}. The closest sample analysed was taken on the April 19th, where EC was 179 μS cm^{-1} and Cl$^-$ was 28.79 mg l^{-1} (Fig. 4d). The average value of the EC in GW3 rose from 107 ± 6 μS cm^{-1} before Experiment 1 to 148 ± 19 μS cm^{-1} after Experiment 1 (Fig. 4c). The second EC peak, following Experiment 2, was lower than the previous year, with a peak value of 176 μS cm^{-1} reached on March 14th 2015. The third rise occurred in late 2015, slowly rising starting in September 21st until its recession in November 11th, with a peak of 207 μS cm^{-1} on October 23rd during a dry period (API7 = 3.5 mm; API30 = 30 mm).

In the stream, EC rose twice on the last 2 days of Experiment 1, April 09th and 10th 2014. Cl$^-$ and Br$^-$ were applied respectively to each of these events (Section 4.1.1). Stream EC started to peak around 1330 on April 09th, 6 h after the well EC started rising. The two stream EC peaks were sharp (both had duration of 4 h between start and fall), and occurred on the only 2 days where shallow lateral flow occurred, respectively 430 and 330 after the shallow lateral flow had initiated (Scaini et al., 2017). The 2 peaks of stream EC were equal to 74.5 and 72.9 μS cm^{-1} respectively. The estimated amount of each peak's Cl$^-$ concentration was respectively 4.09 and 4.02 mg L^{-1} (using the calibration curve between EC and Cl$^-$ described in Section 4.2.3).

The first few natural rainfall events after Experiment 1 did not generate any EC change in the stream (Fig. 4c). In July, between the 11th and the 21st an EC peak was detected at the stream outlet (Fig. 4c). The July peak reached the maximum of stream EC in the whole time series, reaching 145 μS cm^{-1}. The delayed peak in stream EC followed three important summer events: July 6th (16 mm), 8th (16.2 mm) and 9th (21.6 mm), for a total of 53.7 mm in three days (API30 = 48.0 mm; API7 = 9.4 mm). To understand this behaviour, we analyse the events of a similar magnitude (or higher) during the 2 ear period comprising the events.

5.2. Tracer detection

In GW3, Cl$^-$ detection rose from an average value of 5.15 ± 0.42 mg L^{-1} before Experiment 1 to an average value of 7.88 ± 6.64 mg L^{-1} after it (Fig. 4e). This suggests that significant amounts of Cl$^-$ moved through the hillslope and likely reached the stream. The natural presence of Cl$^-$ in stream water does not allow the data to be analysed unambiguously, as the average concentrations before (3.15 ± 0.13 mg L^{-1}) and after (3.22 ± 0.51 mg L^{-1}) the experiments were very similar. Therefore, we focus on Br$^-$ as it was the only tracer that could be used to characterise hillslope response.

Fig. 5 shows cumulative rainfall plotted against cumulative discharge in both 2014 and 2015. In light blue, highlighted by circles, Experiments 1 and 2 are shown. The time where Br$^-$ was detected in GW3 and in SW are highlighted. Br$^-$ was detected on multiple samples in summer 2015: first, it reached SW in detectable quantities during the higher frequency sampling of Experiment 2 (Fig. 4e). Then, it was detected on multiple occasions between May 11th and 13th, June 24th and July 08th, and until September 08th 2015, with rising concentrations. During both summers, the stream was intermittently dry.

With Experiment 1, a total of 5 kg of KBr were released during sprinkling. Through the following months, Br$^-$ was first detected in GW3 starting on June 11th, and was detected in 3 consecutive samples, until beginning of August 2014. Starting from August 20th, Br$^-$ was not detected anymore in the well until Experiment 2, when Br$^-$ was again detected in all samples between March 12th and March 23rd (Fig. 4e). Br$^-$ concentrations in GW3 in this time period were on average 0.30 ± 0.25 mg L^{-1}.

In the stream, Br$^-$ was detected only few months later, on August 06th, 2014. Br$^-$ detection in SW was limited to only 1

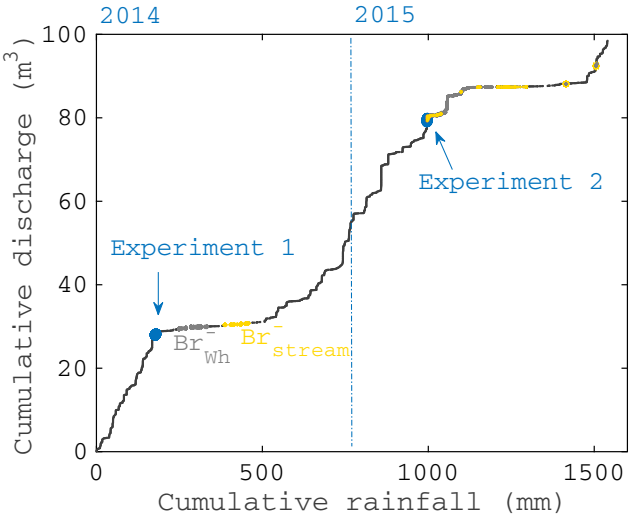

Fig. 5. Cumulative rainfall/cumulative discharge indicating the presence of Br$^-$ in SW (yellow) and GW3 (grey). Light-blue circles show the 2 experiments. A light-blue dashed line indicates the separation between 2014 and 2015. (For interpretation of the references to color in this figure legend, the reader is referred to the web version of this article.)

sample in 2014, with 0.04 mg L^{-1} (the one collected on August 06th). In 2015 Br$^-$ was detected again in the stream, in concentrations of 0.04 ± 0.02 mg L^{-1} (Fig. 4d).

Fig. 6 shows the relationship between GW3 and SW Cl$^-$ (a), SW Cl$^-$ and SW discharge (b), GW3 Cl$^-$ and groundwater depth (c), GW3 Cl$^-$ and GW3 EC (d). The same relationships are shown for Br$^-$ in the right column (Fig. 6e–h). The scatterplots show that Br$^-$ concentrations in SW are ten times lower than in GW3. Br$^-$ was not detected in most of the samples (in SW, only 8 out of the 56 samples following tracer input, Fig. 6f). All the detections corresponded to low water table depth (Fig. 6g) and low flow days (below 5 L s^{-1}), apart from two cases with respectively 8.6 L s^{-1}, on 01/04/2015, and 20.6 L s^{-1}, 03/12/2015 (Fig. 6f). Moreover, Br$^-$ concentrations were detected in SW mostly when the sample occurred on a non-rainy day (Fig. 3). An exception is the last part of 2015, with 2 samples where Br$^-$ was detected on rainfall events lower than 1 m.

Experiment 2 stream sampling showed that there was significant Br$^-$ remobilisation in later events. We observed similar or lower concentrations in the sampling points downstream with respect to 3 other sampling sites located upstream and on the topographical slope (Fig. 1c). At SW, the total of Br$^-$ exported during the 1-month high sampling period during and following Experiment 2 was equal to 125.68 g (2.5% of the total Br$^-$ sprinkled), while the amount of Br$^-$ export in the downstream site was equal to 201.01 g (4.0%). The specific contribution to stream flow during periods of discharge similar to those during the experimental sprinkling (Table 3), estimated using discharge measurements upstream and downstream from the hillslope (total reach length of 10 m), is 0.22 ± 0.14 L s^{-1} (manuscript in preparation).

5.3. Velocity estimates derived from the applied tracers

Estimates of maximum velocity were derived using the double stream EC peak on the last 2 days of Experiment 1 (Section 4.2.4). These estimates were equal to 238 × 10^{-3} m h^{-1} (April 9th) and 208 × 10^{-3} m h^{-1} (April 10th).

The maximum velocity estimated from the start of EC rise at GW3, a few days after the sprinkling, was equal to 191 × 10^{-3} m h^{-1}. The velocity estimated for the peak EC in the well

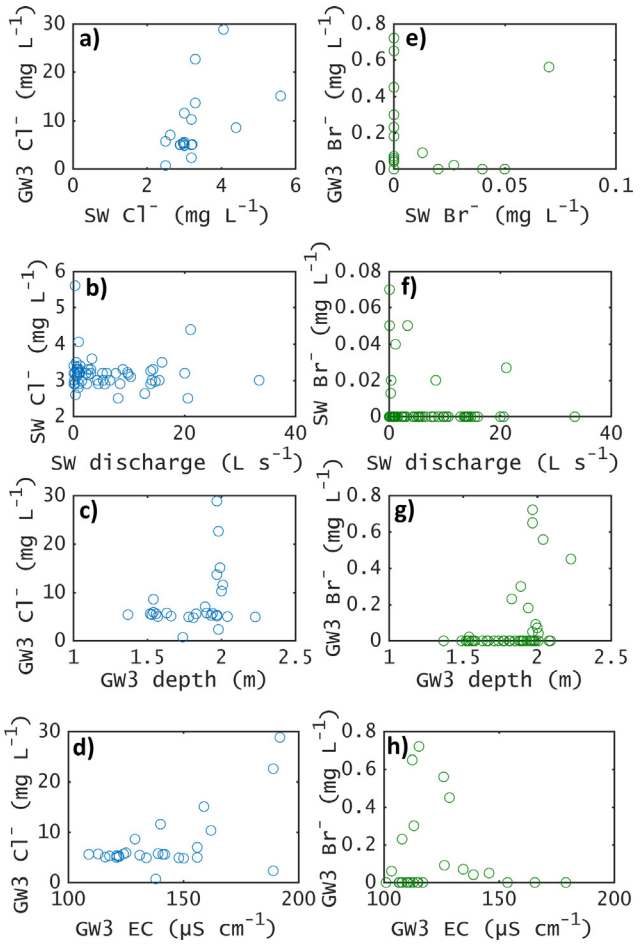

Fig. 6. Scatterplot of the bi-weekly data of 2014 and 2015. Left column: relationship between GW3 and SW Cl^- (a), SW Cl^- and discharge (b), GW3 Cl^- and depth (c), GW3 Cl^- and EC (d). On the right, in green, the same relationships are shown for Br^- (e to h). (For interpretation of the references to color in this figure legend, the reader is referred to the web version of this article.)

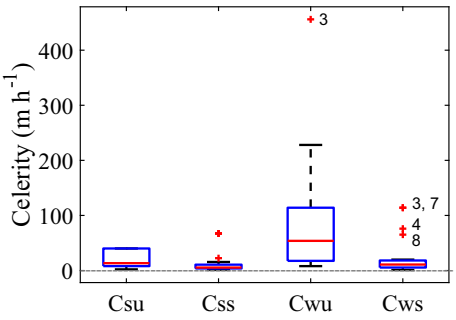

Fig. 7. Box plots showing the range of celerity values obtained for the 21 rainfall events. The x axis shows the celerity type, respectively C_{su}, C_{ss}, C_{wu} and C_{ws}. On each box, the central red mark is the median, the edges of the box are the 25th and 75th percentiles, whilst the black sides show the 5th and 95th percentiles. Red crosses indicate difference >3 standard deviations, with outlier events numbered according to Table 2. (For interpretation of the references to color in this figure legend, the reader is referred to the web version of this article.)

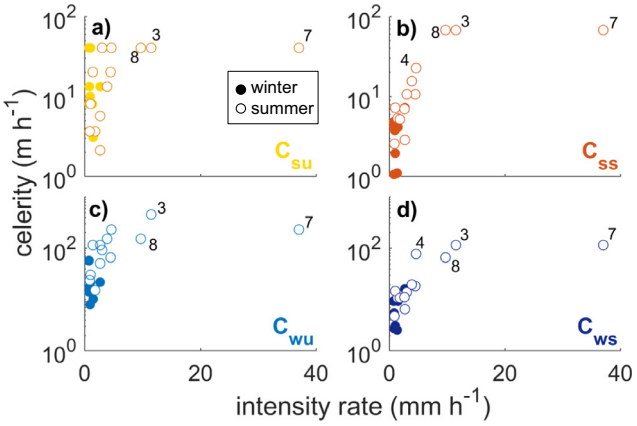

Fig. 8. Estimates of C_{su} (a), C_{ss} (b), C_{wu} (c) and C_{ws} (d) plotted against each event's intensity rate (total rainfall divided by the duration of the event). Filled circles indicate events occurring in the winter (wet) period, while empty circles show summer (dry) period events. Outlier events are numbered according to Table 2.

corresponded to 98×10^{-3} m h^{-1}. On the falling limb of GW3 EC plume, the stream EC described in Section 5.1 was used to estimate a measure of the arrival of the maximum velocity and the mean velocity in connection with the groundwater system, equal to 17.0×10^{-3} m h^{-1} (start of raise) and 15.0×10^{-3} m h^{-1} (corresponding to stream EC peak).

In 2014, the velocity derived from detecting Br^- in SW in the biweekly samples ranged between 16.0 and 14.1×10^{-3} m h^{-1} (calculated respectively for Br^- detected on August 06th and the previous sample on July 24th). In 2015, velocities ranged between 4.9 (March 12th, during Experiment 2) and 2.7×10^{-3} m h^{-1} (December 3rd, the last sample where Br^- was detected).

5.4. Celerity estimates derived from sprinkling and natural events

Fig. 7 shows the box plot of each of the celerity indices estimated using discharge and water table response timings (Section 4.2.5). Celerity values more than 3 standard deviations above the mean are indicated by red crosses and their event number. Event celerities were equal to 19.6 ± 15.2 m h^{-1} (C_{su}) and 15.2 ± 21.8 m h^{-1} (C_{ss}), while hillslope celerities were equal to 89.8 ± 106.2 m h^{-1} (C_{wu}) and 25.2 ± 34.3 m h^{-1} (C_{ws}) (Fig. 7). C_{wu} values were overall much higher than the other estimates, with a maximum of 450 m h^{-1} for event 3 (Fig. 7).

The maximum celerities for all estimates corresponded to the rainfall events that occurred in summer 2014 (event 3, 4, 7 and 8). Event 7 in particular was characterised by the highest intensity rate (37 mm h^{-1}) as 21 mm rained in 30 min, followed by event 3, with an intensity rate of 11 mm h^{-1}. Fig. 8 shows celerity estimates plotted against each event's intensity rate (event intensity/duration) distinguishing dry (summer) and wet (winter) events. Other predictors, such as maximum intensity, rainfall duration, antecedent moisture conditions, and Antecedent Precipitation Index, did not explain the different celerity response.

6. Discussion

6.1. How are groundwater and streamflow dynamics related to rainfall inputs?

The artificial sprinkling experiments did not generate significant hydrometric responses in the GW3 or SW, due to the small amount of sprinkled water on the plot relative to the upslope hillslope area (Section 5.1).

Hydrometric responses in this catchment are comprised of an initial discharge peak coinciding with incident precipitation. Depending on antecedent storage conditions, this peak can occur independently or concurrently with a large, secondary peak – referred to as a double-peak response (Martínez-Carreras et al., 2016). During single-peak events (rainfall > 15 mm), SW discharge peaked in less than 1 h, while the water table measured at GW3 reacted after the discharge peak. At the same time, maximum

cross-correlations between rainfall and discharge in single-peak events were always greater than the maximum cross-correlations between rainfall and water table (Table 2), indicating that discharge and rainfall were better correlated during single-peak events greater than 15 mm. The delayed hillslope runoff response, relative to that of streamflow, has been observed in other studies (Harr, 1977; Montgomery et al., 1997; Penna et al., 2015; Turton et al., 1992; Weyman, 1970). This suggests a complexity in the groundwater response time in comparison to discharge, and suggests delayed recharge to the water table from the unsaturated zone over most of the catchment area – except perhaps in near saturated riparian areas (considering that the first peak is indeed primarily event water as proposed by Jackisch et al., 2016; Wrede et al., 2015).

The cross-correlation analysis suggests that the hillslope response in some cases may be controlled by a storage threshold rather than rainfall characteristics (Gannon et al., 2014; Graham et al., 2010; Tromp-van Meerveld and McDonnell, 2006). The computed cross-correlations using time-series from double-peak events show that there is a mechanism of release of water that is activated when the depth to groundwater reaches to within 1.6–1.5 m of the soil surface for rainfall events of more than 15 mm. Above this limit, the water table triggers a connection to the stream within a time frame of 1–3 h. Such connection is demonstrated by the correlation of the second, lagged, discharge rise to water table dynamics, rather than to rainfall. Such cases could be defined as storage-driven discharge peaks, and correspond to the second type of peak response described in Martínez-Carreras et al. (2016).

In the case of the storage-driven double-peak events, cross-correlation analysis suggests the first peak can be seen as rainfall-driven, as the maximum correlation to rainfall is similar to correlation coefficients among single-peak events (Section 5.1). Some events exhibit a general poor correlation among rainfall, discharge and water table dynamics (event 12 and 21, double peak events characterised by long rainfall duration and low intensity, Table 2); this is likely due to composite rainfall-driven and storage-driven discharge peaks, which are more difficult to evaluate with the cross-correlation technique.

The rising of the water table at the hillslope base concomitantly – or before – discharge increase is a common perception of hillslope groundwater contributions (Kim et al., 2004; Mosley, 1979; Sklash and Farvolden, 1979). The different temporal response observed here between groundwater and streamflow in the rainfall-driven and storage-driven peaks indicates a more complex non-linear hillslope response (McGuire and McDonnell, 2010) and helps demonstrate the dependence of the runoff on storage as shown in Martínez-Carreras et al. (2016).

6.2. Tracer transport between plot and stream

6.2.1. Groundwater response

The amounts of Cl^- and Br^- sprinkled during the 2 experiments were detected in both GW3 and SW at different times (Section 5.2). In GW3, a rise in water table corresponded to a decrease in EC, indicating dilution, whilst a decrease in water table corresponded to a rise in EC value, indicating higher concentrations (Fig. 4).

The tracers stored in the subsurface are likely responsible for the EC rise in GW3, as EC is an indicator for dissolved ions (Hayashi, 2004). Previous work at the plot scale from soil analysis performed in autumn 2014 (after Experiment 1 was carried out) showed that significant amounts of Cl^- and Br^- stored in the soil were likely remobilised during rainfall events, and that such remobilisation was more pronounced in the case of heavy summer events (Scaini et al., 2017). Unpublished additional laboratory experiments established that the soil of the studied hillslope has the potential to retain on average about 30% and 25% of Cl^- and Br^-, respectively (Fig. SI-1). They also show that the stored tracers cannot be totally removed from the soil matrix during successive leaching experiments, and about 10% of both tracers could be suspected to stay for a longer term (Fig. SI-2). An interesting consequence of this behaviour is shown by the third peak in the water table EC (Fig. 4c). During one of the driest months of the series, October 2015 (<30 mm rainfall), the water table level was low (1.9 m below the surface) and stable. Under these conditions, well EC exhibited its highest value for the entire two-year series (207 $\mu S\ cm^{-1}$ on October 23rd). However, the groundwater level readings between September and November 2015 are suspect of malfunctioning of the instrument, because the water level does not decrease during a period without rainfalls. As the EC ofthe water table is recorded by the same instrument, we cannot yet make a sound interpretation of this late rise of EC because it might be caused by an instrumental error.

6.2.2. Stream response

An inverse relationship between EC and discharge linked to dilution was also observed in the stream data and has been documented by others (Kobayashi, 1986). In support of this interpretation, Br^- was detected in the stream measurement points only on low-flow days (Fig. 6), when stream chemistry was not diluted with water from rainfall events. The only stream Br^- sample that was detected during high discharge (20.6 $L\ s^{-1}$) was also the only sample containing detectable Br^-. This event occurred after a long period of low flow ($0.31 \pm 0.25\ L\ s^{-1}$). Unfortunately, stream EC was not available during such a time period (Fig. 4).

The reason for stream EC rise during low flows and heavy summer events in 2014 could be due to groundwater fluxes, releasing in the stream the high-EC water containing tracers. In wet conditions, such contribution could be not detected because of its minor contribution to catchment-scale runoff generation, as we do observe little Br^- in the stream during rainfall events. The tracer detection in the stream only under low-flow conditions does not mean that there is no Br^- during high flows. Tracer flux may increase during high flows but the increase may still not achieve concentrations above the detection limit, as this hillslope, with an upslope accumulating area of 3 ha, represents a small fraction of the total catchment area (46 ha).

6.3. How do bedrock structural properties influence tracer transport from plot to stream?

Recent studies have recognized the importance of identifying runoff generating mechanisms governed by fractured bedrock hydrogeology (Banks et al., 2009; Hale et al., 2016). In the Weierbach, limited information has been available to date to understand the extent that fractured bedrock can influence subsurface flow dynamics. Our set-up allowed us to investigate whether water from the hillslope during events moved along the bedrock cleavage plans or along the predominant slope angle (Fig. 1.c). Differences in concentration between the stream sampling points show a clear increase in the downslope sampling points with respect to the sampling point located along the predominant slope angle. This suggests that the predominant flowpath direction follows the bedrock cleavage and not the surface slope. Mass flux estimates of Br^-export were higher at the furthest downstream measurement point (4% of input) relative to SW, the stream outlet (2.5% of input); Br^- was detected only twice directly downstream from the hillslope (Section 5.2).

Unfortunately, the two wells located at the bottom of the experimental plot, GW1 and GW2, were dry throughout the observation period and do not provide useful information other than to further reinforce the heterogeneous nature of the bedrock.

With the available data we cannot query whether the tracer plume moved further downstream than the strike had suggested (i.e. did more tracer reach the stream at angles greater than the bedrock cleavage?). Our data suggest the possibility that groundwater flow was dominated by a downslope gradient different from the surface slope. Such a possibility is described in Fig. 9, where arrows indicate the prevalent flow direction in the soil layer (vertical) and bedrock (laterally oriented fractures, due to cleavage). This 2-layered structure suggests that the deeper groundwater body, within the bedrock, would also cause the catchment area to differ from its topographical approximation. The importance of the subsurface boundaries have been recently discussed in hydrological studies: Hale et al., (2016) identified subsurface permeability structure as the main control on water storage and release. In another study, fractured sedimentary bedrock were responsible for the rapid response of bedrock groundwater at the hillslope scale (Padilla et al., 2014) and resultant generated runoff (Padilla et al., 2015). Pfister et al. (2017) have documented bedrock geological controls on catchment storage, mixing and release in a set of 16 nested catchments in Luxembourg. In our study we could not locate the maximum depth to which groundwater storage extends, but we did manage to identify a structure that controls flow direction through the cleavage orientation, and demonstrated its importance in directing hillslope runoff. In this catchment, a component of flow through the bedrock could also control a larger component of the water balance (as was the case in Panola, Tromp-van Meerveld et al., 2007).

Our hillslope-scale experiment showed that, in the case of fractured systems like the Weierbach catchment, not only bedrock topography but also the cleavage controls the release of water to the stream. Our findings are valid for rainfall events greater than 15 m, as large amounts of water were sprinkled on a 64^2 plot (Section 4.1), during relatively dry antecedent conditions across the catchment. More generally, we suggest that in addition to accounting for flow that occurs at the bedrock and soil interface, we should also recognize the importance of the cleavage orientation to correctly characterise and predict the fracture contributions to runoff.

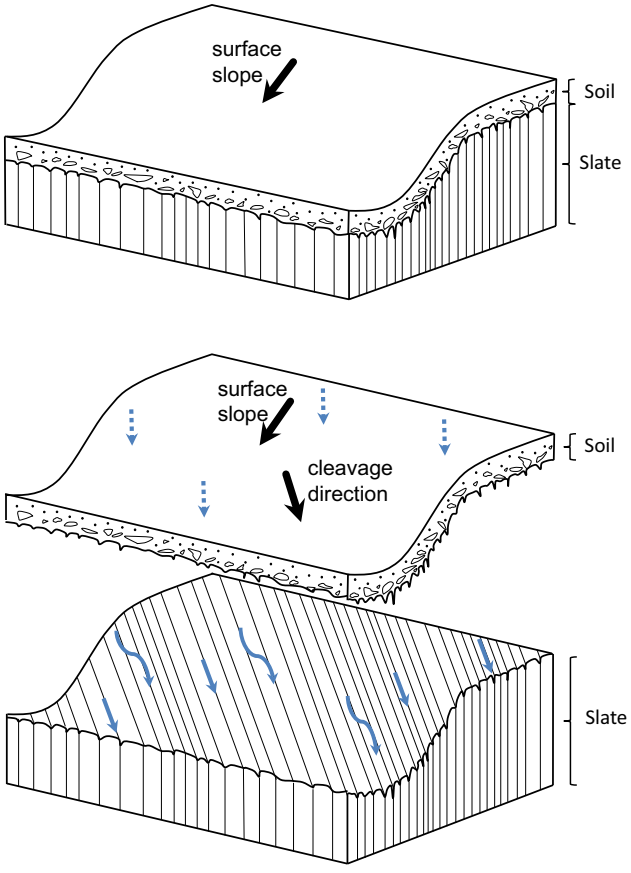

Fig. 9. Sketch of the studied hillslope indicating the prevalent flow direction following the prevalent bedrock cleavage direction. Tracer arrival to the river shows evidence for a diagonal prevalent direction of flow from the plot.

6.4. How does tracer transport relate to estimates of celerities?

Being able to estimate both celerity and velocity responses is an important step toward determining dynamic storage variability, which controls both the hydrometric stream flow response, and the storage that regulates solute transport (Beven, 2012; Birkel and Soulsby, 2015; Davies and Beven, 2015).

The integral celerity responses estimated for natural rainfall events were characterised by values within the 25th and 75th percentiles, except for a few cases with exceptionally high values, while the initial estimates were more variable, particularly in the hillslope response (Fig. 7). The heterogeneity of our celerity estimates reflects the complexity of the response of the catchment (Figs. 7 and 8). The differences between initial and integral response of our estimates, refer to the combination of different processes that are likely involved in the responses (Iorgulescu et al., 2007; McDonnell et al., 2010; Reeves et al., 1996).

The highest celerities, observed during events characterised by high intensity and short duration, were observed during June and July of 2014: events 3, 4, 7 and 8 in Table 2 (Fig. 7). The highest celerities corresponded to summer events where the intensity rate was the highest, suggesting an influence of both event intensity and residual storage (summer, warm conditions) on celerity responses. In such a system, a higher rainfall rate would generate a faster response in the unsaturated zone once a storage threshold has been exceeded, resulting in a quicker celerity. The importance of unsaturated zone dynamics in the hydrologic response was suggested in early studies in permeable soils (Torres et al., 1998) and could explain the maximum initial celerities being higher than the integral celerities (Barnard et al., 2010). We observed a seasonality effect in the intensity rate/celerity response of Fig. 8: a 20-mm event in summer generates a higher impact on the residual storage of water than the same intensity in winter, as such water quantity would be diluted within the (higher) winter residual storage. In turn, antecedent conditions (in terms of API7, API30 and antecedent moisture) of the correspondent rainfall event did not contribute to explain the high celerity values.

The hillslope set-up included continuous measurement of water table depth and streamflow as well as EC monitoring and water sampling allowing for a comparison between velocities and celerities. In comparison to the celerity, the maximum velocity values (indicated by a grey dotted line in Fig. 7) were always below 1 m h^{-1}, in the same range of the lower celerities derived from the natural events (equal to 0.9–1.1 m h^{-1}).

Small amounts of shallow lateral preferential flow were observed at the sprinkler plot throughflow trenches at depths of 25 and 50 cm in the work of Scaini et al. (2017). For these flows the maximum vertical velocities estimated for the tracers were variable and ranged as high as $677 \pm 420 \times 10^{-3}$ m h^{-1}, whilst celerities were as high as $971 \pm 625 \times 10^{-3}$ m h^{-1}. At the plot scale, the highest measured maximum velocity was equal to 1.2 h^{-1}. Here, we estimated the maximum velocities at the hillslope scale, as estimated by the two EC peaks recorded in SW (238 and 208 $\times$ 10^{-3} m h^{-1}), and found that they are higher than maximum velocity in GW3 (191×10^{-3} m h^{-1}), suggesting possible preferential flow pathways (Sections 5.3 and 6.1). The EC peaks are not high in magnitude, as increase in EC to 74.5 would correspond to a concentration of Cl^- of 4.09 mg L^1 (Section 4.2.3), and do not suggest a

significant volume of tracer reaching the water table (though no sample was available on those dates). These maximum velocities suggest that preferential flowpaths may allow for the hillslope to contribute to the first discharge peak. Under the experimental conditions (dry antecedent conditions, and artificial sprinkling on the 64^2 plot only, Table 3), it is possible that preferential flow along the hillslope may not reach deep enough to instigate a downslope response (see for example, Germann (2014)).

The estimate of maximum velocity to the stream following the groundwater well peak, $V_{max,ws}$, both estimated by EC data (17.0×10^{-3} m h^{-1}) and Br^- detection (14.0 and 16.0×10^{-3} m h^{-1}) were in agreement with each other given the sparse sampling interval (Section 4.2.4). The movement of tracer in the soil is complex, with Br^- involved in remobilisation processes as demonstrated by the high sampling stream set-up during and after Experiment 2. Additionally, we only calculated sample means, with additional issues about (i) flux weighting as we detect concentrations but not fluxes at the well, and (ii) dilution at the stream to concentrations below detection limit (with the possibility of incomplete mixing with the stream water). Such problems in tracing preferential pathways and sources in fractured bedrock systems have been encountered by others (Genereux et al., 1993; Shand et al., 2007).

7. Conclusions

This study analysed the subsurface flow pathways in the Weierbach catchment (Luxembourg). The peculiarity of this catchment is that it is underlain by slate bedrock, which is orientated in a preferential direction. A major focus of this work was to understand the influence of this anisotropy on subsurface processes.

Sprinkling experiments were designed to infer subsurface flow pathways. In particular, tracer concentrations were monitored at multiple sites through the stream and in a well located along the main direction of the bedrock cleavage. Estimates of hillslope and hydrograph celerities were calculated using water table and discharge responses respectively.

Our main research questions are (i) How are groundwater and streamflow dynamics related to rainfall inputs? (ii) How do bedrock characteristic, including orientation of the fractures, influence tracer transport from plot to stream? (iii) How does tracer transport relate to estimates of celerities?

From the combined hydrometric and chemical analyses, we managed to provide answers to our specific questions.

- For natural rainfall events of more than 15 mm there is a difference between the mechanisms controlling the rainfall-driven (single or first peaks in double peak events) and storage-driven (second peak in double peak events) discharge peaks, supporting recent work undertaken by Martínez-Carreras et al. (2016). Our results suggest that rainfall rate and residual storage present a seasonality effect and are the primary controls on celerity responses.
- The characteristics of our site suggested that bedrock structural properties as cleavage orientation control flow direction, as subsurface flowpaths were in line with the orientation of the bedrock fractures.
- Combining velocity and celerity estimates we suggest that there could be a fast flowpath component connecting the hillslope to the stream, but velocity information was too scarce to prove such a hypothesis, as velocity estimates were largely lower than celerities.

This study has suggested the importance of fracture orientation in subsurface flow generation in forested catchments. In particular, cleavage orientation is important in determining the catchment area contributing to runoff, which may differ significantly from the contributing area determined based on topography.

Acknowledgments

Research funded by National Research Fund of Luxembourg (FNR) core project ECSTREAM (C12/SR/4018854). François Barnich and Delphine Collard are thanked for the chemical analysis. Laura Giustarini, Audrey Campeau and Marta Antonelli are thanked for assistance with data analysis. Jay Frentress and Nino Amvrosiadi are thanked for edits on an early version of the manuscript.

Appendix A. Supplementary data

Supplementary data associated with this article can be found, in the online version, at https://doi.org/10.1016/j.jhydrol.2017.12.011.

References

Abbott, B.W., Baranov, V., Mendoza-Lera, C., Nikolakopoulou, M., Harjung, A., Kolbe, T., Balasubramanian, M.N., Vaessen, T.N., Ciocca, F., Campeau, A., Wallin, M.B., Romeijn, P., Antonelli, M., Gonçalves, J., Datry, T., Laverman, A.M., de Dreuzy, J. R., Hannah, D.M., Krause, S., Oldham, C., Pinay, G., 2016. Using multi-tracer inference to move beyond single-catchment ecohydrology. Earth-Sci. Rev. https://doi.org/10.1016/j.earscirev.2016.06.014.

Banks, E.W., Simmons, C.T., Love, A.J., Cranswick, R., Werner, A.D., Bestland, E.A., Wood, M., Wilson, T., 2009. Fractured bedrock and saprolite hydrogeologic controls on groundwater/surface-water interaction: a conceptual model (Australia). Hydrogeol. J. 17, 1969–1989. https://doi.org/10.1007/s10040-009-0490-7.

Barnard, H.R., Graham, C.B., Verseveld, W.J. Van, Brooks, J.R., Bond, B.J., McDonnell, J. J., 2010. Mechanistic assessment of hillslope transpiration controls of diel subsurface flow: a steady-state irrigation approach. Ecohydrology 3, 133–142. https://doi.org/10.1002/eco.114.

Beven, K., 2012. The Primer, Rainfall-Runoff Modelling. John Wiley & Sons, Ltd.. 10.1002/9781119951001.

Beven, K., 1981. Kinematic subsurface stormflow. Water Resour. Res. 17, 1419–1424. https://doi.org/10.1029/WR017i005p01419.

Beven, K., Germann, P., 1982. Macropores and water flow in soils. Water Resour. Res. 18, 1311–1325. https://doi.org/10.1029/WR018i005p01311.

Beven, K.J., 2010. Preferential flows and travel time distributions: Defining adequate hypothesis tests for hydrological process models. Hydrol. Process. 24, 1537–1547. https://doi.org/10.1002/hyp.7718.

Beven, K.J., 2006. Streamflow Generation Processes, Selection, Introduction and Commentary.

Birkel, C., Soulsby, C., 2015. Advancing tracer-aided rainfall-runoff modelling: a review of progress, problems and unrealised potential. Hydrol. Process. 29, 5227–5240. https://doi.org/10.1002/hyp.10594.

Bryan, R.B., Jones, J.A.A., 1997. The significance of soil piping processes: inventory and prospect. Geomorphology 20, 209–218. https://doi.org/10.1016/S0169-555X(97)00024-X.

Chang, C., Sommerfeldt, T.G., Carefoot, J.M., Schaalje, G.B., 1983. Relationships of electrical conductivity with total dissolved salts and cation concentration of sulfate-dominant soil extracts. Can. J. soil Sci. 63, 79–86.

Chappell, N.A., 2010. Soil pipe distribution and hydrological functioning within the humid tropics: a synthesis. Hydrol. Process. 24, 1567–1581. https://doi.org/10.1002/hyp.7579.

Chappell, N.A., Sherlock, M., Bidin, K., Macdonald, R., 2007. Runoff processes in Southeast Asia: role of soil, regolith, and rock type. For. Environ. Mekong River Basin, 3–23.

Cook, P.G., Land, C., Osmond, G., 2003. A guide to regional flow in fractured rock aquifers. Water 115.

Cook, P.G., Solomon, D.K., Sanford, W.E., Busenberg, E., Plummer, L.N., Poreda, R.J., 1996. Inferring shallow groundwater flow in saprolite and fractured rock using environmental tracers. Water Resour. Res. 32, 1501–1509. https://doi.org/10.1029/96WR00354.

Davies, J., Beven, K., Nyberg, L., Rodhe, A., 2011. A discrete particle representation of hillslope hydrology: hypothesis testing in reproducing a tracer experiment at Gårdsjön Sweden. Hydrol. Process. 25, 3602–3612. https://doi.org/10.1002/hyp.8085.

Davies, J., Beven, K.J., 2012. Comparison of a Multiple Interacting Pathways model with a classical kinematic wave subsurface flow solution. Hydrol. Sci. J. 57, 203–216.

Davies, J.A.C., Beven, K., 2015. Hysteresis and scale in catchment storage, flow and transport. Hydrol. Process. 29, 3604–3615. https://doi.org/10.1002/hyp.10511.

Dunne, T., 1978. Field studies of hillslope flow processes. In: Kirkby, M. (Ed.), Hillslope Hydrology. John Wiley & Sons, pp. 227–293.

Eggleton, R.A., 2001. The Regolith Glossary, CRC LEME.

Gabrielli, C.P., McDonnell, J.J., Jarvis, W.T., 2012. The role of bedrock groundwater in rainfall-runoff response at hillslope and catchment scales. J. Hydrol. 450–451, 117–133. https://doi.org/10.1016/j.jhydrol.2012.05.023.

Gannon, J.P., Bailey, S.W., McGuire, K.J., 2014. Organizing groundwater regimes and response thresholds by soils: A framework for understanding runoff generation in a headwater catchment. Water Resour. Res. 8403–8419. https://doi.org/10.1002/2014WR015498.Received.

Genereux, D.P., Hemond, H.F., Mulholland, P.J., 1993. Use of radon-222 and calcium as tracers in a three-end-member mixing model for streamflow generation on the West Fork of Walker Branch Watershed. J. Hydrol. 142, 167–211. https://doi.org/10.1016/0022-1694(93)90010-7.

Germann, P.F., 2014. Preferential Flow—Stokes Approach to Infiltration and Drainage, Geographica Bernensia. University of Bern, Bern.

Gilman, K., Newson, M.D., 1980. Soil pipes and pipeflow, a hydrological study in upland Wales. BGRG Res. Monogr. 1, 1444–1454.

Graham, C.B., Woods, R., a., McDonnell, J.J.,, 2010. Hillslope threshold response to rainfall: (1) A field based forensic approach. J. Hydrol. 393, 65–76. https://doi.org/10.1016/j.jhydrol.2009.12.015.

Hale, C., McDonnell, J.J., 2016. Effect of bedrock permeability on stream base flow Catchment, transit time scaling relations: 1. A multiscale. Intercomparison 52, 1358–1374. https://doi.org/10.1002/2014WR016124.

Hale, V.C., McDonnell, J.J., Stewart, M.K., Solomon, D.K., Doolitte, J., Ice, G.G., Pack, R. T., 2016. Effect of bedrock permeability on stream base flow mean transit time scaling relationships: 2. Process study of storage and release. Water Resour. Res. 51, 9127–9140. https://doi.org/10.1002/2014WR016259.

Harr, R.D., 1977. Water flux in soil and subsoil on a steep forested slope. J. Hydrol. 33, 37–58. https://doi.org/10.1016/0022-1694(77)90097-X.

Hayashi, M., 2004. Temperature-electrical conductivity relation of water for environmental monitoring and geophysical data inversion. Environ. Monit. Assess. 96, 119–128. https://doi.org/10.1023/B:EMAS.0000031719.83065.68.

Hewlett, J.D., Hibbert, A.R., 1967. Factors affecting the response of small watersheds to precipitation in humid areas. For. Hydrol. 275–290. https://doi.org/10.1177/030913330933811 8.

Iorgulescu, I., Beven, K.J., Musy, A., 2007. Flow, mixing, and displacement in using a data-based hydrochemical model to predict conservative tracer data. Water Resour. Res. 43, 1–12. https://doi.org/10.1029/2005WR004019.

Jackisch, C., Angermann, L., Allroggen, N., Sprenger, M., Blume, T., Weiler, M., Tronicke, J., Zehe, E., 2016. In situ investigation of rapid subsurface flow: Identification of relevant spatial structures beyond heterogeneity. Hydrol. Earth Syst. Sci. Discuss. 1–32. https://doi.org/10.5194/hess-2016-190.

Jackson, C.R., 1992. Hillslope infiltration and lateral downslope unsaturated flow. Water Resour. Res. 28, 2533–2539. https://doi.org/10.1029/92WR00664.

Jones, J., Crane, F., 1984. Pipeflow and pipe erosion in the Maesnant experimental catchment. In: Burt, T., Walling, D. (Eds.), Catchment Experiments in Fluvial Geomorphology. UBC Press, Norwich, pp. 55–72.

Juilleret, J., Dondeyne, S., Vancampenhout, K., Deckers, J., Hissler, C., 2016. Mind the gap: a classification system for integrating the subsolum into soil surveys. Geoderma. https://doi.org/10.1016/j.geoderma.2015.08.031.

Juilleret, J., Iffly, J.F., Pfister, L., Hissler, C., 2011. Remarkable Pleistocene periglacial slope deposits in Luxembourg (Oesling): pedological implication and geosite potential. Bull. la Société des Nat. Luxemb. 112, 125–213.

Kim, H.J., Sidle, R.C., Moore, R.D., Hudson, R., 2004. Throughflow variability during snowmelt in a forested mountain catchment, coastal British Columbia Canada. Hydrol. Process. 18, 1219–1236. https://doi.org/10.1002/hyp.1396.

Klaus, J., Chun, K.P., McGuire, K.J., McDonnell2, J.J.,, 2015. Temporal dynamics of catchment transit times from stable isotope data. Water Resour. Res. 51, 4208–4223. https://doi.org/10.1016/0022-1694(68)90080-2.

Kobayashi, D., 1986. Separation of a snowmelt hydrograph by stream conductance. J. Hydrol. 84, 157–165. https://doi.org/10.1016/0022-1694(86)90049-1.

Laine-Kaulio, H., Backnäs, S., Karvonen, T., Koivusalo, H., McDonnell, J.J., 2014. Lateral subsurface stormflow and solute transport in a forested hillslope: a combined measurement and modeling approach. Water Resour. Res. 50, 8159–8178. https://doi.org/10.1002/2014wr015381.

Lorz, C., Heller, K., Kleber, A., 2011. Stratification of the regolith continuum – a key property for processes and functions of landscapes. Z. Geomorphol. 55, 277–292. https://doi.org/10.1127/0372-8854/2011/0055S3-0062. Suppl. Issues.

Martínez-Carreras, N., Hissler, C., Gourdol, L., Klaus, J., Juilleret, J., François Iffly, J., Pfister, L., 2016. Storage controls on the generation of double peak hydrographs in a forested headwater catchment. J. Hydrol. https://doi.org/10.1016/j.jhydrol.2016.10.004.

McDonnell, J.J., Beven, K.J., 2014. Debates—The future of hydrological sciences: a (common) path forward? A call to action aimed at understanding velocities, celerities and residence time distributions of the headwater hydrograp. Water Resour. Res. 50, 5342–5350. https://doi.org/10.1002/2013WR015141.Received.

McDonnell, J.J., McGuire, K., Aggarwal, P., Beven, K.J., Biondi, D., Destouni, G., Dunn, S., James, A., Kirchner, J., Kraft, P., Lyon, S., Maloszewski, P., Newman, B., Pfister, L., Rinaldo, A., Rodhe, A., Sayama, T., Seibert, J., Solomon, K., Soulsby, C., Stewart, M., Tetzlaff, D., Tobin, C., Troch, P., Weiler, M., Western, A., Wörman, A., Wrede, S., 2010. How old is streamwater? Open questions in catchment transit time conceptualization, modelling and analysis. Hydrol. Process. 24, 1745–1754. https://doi.org/10.1002/hyp.7796.

McGuire, K.J., McDonnell, J.J., 2010. Hydrological connectivity of hillslopes and streams: Characteristic time scales and nonlinearities. Water Resour. Res. 46, n/a–n/a. doi:10.1029/2010WR009341.

McGuire, K.J., Weiler, M., McDonnell, J.J., 2007. Integrating tracer experiments with modeling to assess runoff processes and water transit times. Adv. Water Resour. 30, 824–837. https://doi.org/10.1016/j.advwatres.2006.07.004.

Montgomery, D.R., Dietrich, W.E., Torres, R., Anderson, S.P., Heffner, J.T., Loague, K., 1997. Hydrologic response of a steep, unchanneled valley to natural and applied rainfall. Water Resour. Res. 33, 91–109. https://doi.org/10.1029/96WR02985.

Moragues Quiroga, C., Juilleret, J., Gourdol, L., Pelt, E., Perrone, T., Aubert, A., Morvan, G., Legout, A., Stille, P., Hissler, C., 2017. Genesis and evolution of regoliths: evidence from trace and major elements and Sr-Nd-Pb-U radiogenic isotopes. Catena 149, 185–198.

Mosley, M.P., 1979. Streamflow generation in a forested watershed, New Zealand. Water Resour. Res. 15, 795–806. https://doi.org/10.1029/WR015i004p00795.

Nyberg, L., Rodhe, A., Bishop, K., 1999. Water transit times and flow paths from two line injections of 3H and 36Cl in a microcatchment at Gårdsjön Sweden. Hydrol. Process. 13, 1557–1575. https://doi.org/10.1002/(sici)1099-1085(19990815)13:11<1557::aid-hyp835>3.0.co;2-s.

Onda, Y., Komatsu, Y., Tsujimura, M., Fujihara, J.I., 2001. The role of subsurface runoff through bedrock on storm flow generation. Hydrol. Process. 15, 1693–1706. https://doi.org/10.1002/hyp.234.

Padilla, C., Onda, Y., Iida, T., 2015. Interaction between runoff - bedrock groundwater in a steep headwater catchment underlain by sedimentary bedrock fractured by gravitational deformation. Hydrol. Process. 29, 4398–4412. https://doi.org/10.1002/hyp.10498.

Padilla, C., Onda, Y., Iida, T., Takahashi, S., Uchida, T., 2014. Characterization of the groundwater response to rainfall on a hillslope with fractured bedrock by creep deformation and its implication for the generation of deep-seated landslides on Mt. Wanitsuka Kyushu Island. Geomorphology 204, 444–458. https://doi.org/10.1016/j.geomorph.2013.08.024.

Penna, D., van Meerveld, H.J., Oliviero, O., Zuecco, G., Assendelft, R.S., Dalla Fontana, G., Borga, M., 2015. Seasonal changes in runoff generation in a small forested mountain catchment. Hydrol. Process. 29, 2027–2042. https://doi.org/10.1002/hyp.10347.

Pfister, L., Martínez-Carreras, N., Hissler, C., Klaus, J., Carrer, G.E., Stewart, M.K., McDonnell, J.J., 2017. Bedrock geology controls on catchment storage, mixing and release: a comparative analysis of 16 nested catchments. Hydrol. Process. https://doi.org/10.1002/hyp.11134.

Rasmussen, T.C., Baldwin, R.H., Dowd, J.F., Williams, A.G., 2000. Tracer vs. pressure wave velocities through unsaturated saprolite. Soil Sci. Soc. Am. J. 64, 75. https://doi.org/10.2136/sssaj2000.64175x.

Reeves, A.D., Anderson, M.C., Beven, K., 1996. Flow separation in undisturbed soils using multiple anionic tracers. Part 1. Analytical methods and unsteady rainfall and return flow experiments. Hydrol. Process. 10, 1435–1450. 0885-6087/96/111435-16.

Scaini, A., Audebert, M., Hissler, C., Fenicia, F., Gourdol, L., Pfister, L., Beven, K., 2017. Velocity and celerity dynamics at plot scale inferred from artificial tracing experiments and time-lapse ERT. J. Hydrol. 546, 28–43. https://doi.org/10.1016/j.jhydrol.2016.12.035.

Scudeler, C., Pangle, L., Pasetto, D., Niu, G.-Y., Volkmann, T., Paniconi, C., Putti, M., Troch, P., 2016. Multiresponse modeling of an unsaturated zone isotope tracer experiment at the Landscape Evolution Observatory. Hydrol. Earth Syst. Sci. Discuss. 1–29. https://doi.org/10.5194/hess-2016-228.

Shand, P., Darbyshire, D.P.F., Gooddy, D., Haria, H., A.,, 2007. 87Sr/86Sr as an indicator of flowpaths and weathering rates in the Plynlimon experimental catchments, Wales, U.K. Chem. Geol. 236, 247–265. https://doi.org/10.1016/j.chemgeo.2006.09.012.

Sidle, R.C., Tsuboyama, Y., Noguchi, S., Hosoda, I., Fujieda, M., Shimizu, T., 1995. Seasonal hydrologic response at various spatial scales in a small forested catchment, Hitachi Ohta. Japan. J. Hydrol. 168, 227–250. https://doi.org/10.1016/0022-1694(94)02639-S.

Singhal, B.B.S., Gupta, R.P., 2010. Applied Hydrogeology of Fractured Rocks, 2nd ed., Netherlands. doi:10.1007/978-90-481-8799-7.

Siosemarde, M., Kave, F., Pazira, E., Sedghi, H., Ghaderi, S.J., 2010. Determine of constant coefficients to relate total dissolved solids to electrical conductivity. Aust. J. Soil Res. 4, 258–260.

Sklash, M.G., Farvolden, R.N., 1979. The role of groundwater in storm runoff. J. Hydrol. 43, 45–65.

Soulsby, C., Birkel, C., Geris, J., Dick, J., Tunaley, C., Tetzlaff, D., 2015. Stream water age distributions controlled by storage dynamics and nonlinear hydrologic connectivity: modeling with high-resolution isotope data. Water Resour. Res. 51, 7759–7776. https://doi.org/10.1002/2015WR017888.

Torres, R., Dietrich, W.E., Montgomery, D.R., Anderson, S.P., Loague, K., 1998. Unsaturated zone processes and the hydrologic response of a steep, unchanneled catchment. Water Resour. Res. 34, 1865. https://doi.org/10.1029/98WR01140.

Tromp-van Meerveld, H.J., McDonnell, J.J., 2006. Threshold relations in subsurface stormflow: 2. The fill and spill hypothesis. Water Resour. Res. 42, n/a–n/a. doi:10.1029/2004WR003800.

Tromp-van Meerveld, H.J., Peters, N.E., McDonnell, J.J., 2007. Effect of bedrock permeability on subsurface stormflow and the water balance of a trenched hillslope at the Panola Mountain Research Watershed, Georgia USA. Hydrol. Process. 21, 750–769. https://doi.org/10.1002/hyp.

Trudgill, S.T., Pickles, A.M., Smettem, K.R.J., 1983. Soil-water residence time and solute uptake: 2. Dye tracing and preferential flow predictions. J. Hydrol. 62, 279–285. doi: 10.1016/0022-1694(83)90107-5.

Turton, D.J., Haan, C.T., Miller, E.L., 1992. Subsurface flow responses of a small forested catchment in the Ouachita Mountains. Hydrol. Process. 6, 111–125. https://doi.org/10.1002/hyp.3360060110.

Uchida, T., Tromp-van Meerveld, H.J., McDonnell, J.J., 2005. The role of lateral pipe flow in hillslope runoff response: an intercomparison of non-linear hillslope response. J. Hydrol. 311, 117–133. https://doi.org/10.1016/j.jhydrol.2005.01.012.

Weihermüller, L., Siemens, J., Deurer, M., Knoblauch, S., Rupp, H., Göttlein, A., Pütz, T., 2007. In situ soil water extraction: a review. J. Environ. Qual. 36, 1735–1748. https://doi.org/10.2134/jeq2007.0218.

Weyman, D.R., 1973. Measurements of the downslope flow of water in a soil. J. Hydrol. 20, 267–288. https://doi.org/10.1016/0022-1694(73)90065-6.

Weyman, D.R., 1970. Throughflow on hillslopes and its relation to the stream hydrograph. Bull. Int. Assoc. Sci. Hydrol. 15, 25–33. doi:10.1080/02626667009493969.

Whipkey, R.Z., 1965. Subsurface stormflow from forested hillslopes. Int. Assoc. Sci. Hydrol. Bull. 10, 74–85. https://doi.org/10.1080/02626666509493392.

Wienhöfer, J., Zehe, E., 2014. Predicting subsurface stormflow response of a forested hillslope – the role of connected flow paths. Hydrol. Earth Syst. Sci. 18, 121–138. https://doi.org/10.5194/hess-18-121-2014.

WRB, I.W.G., 2015. World Reference Base for Soil Resources 2015: international soil classification system for naming soils and creating legends for soil maps., In: World Soil Resources Reports. FAO, Rome.

Wrede, S., Fenicia, F., Martínez-Carreras, N., Juilleret, J., Hissler, C., Krein, A., Savenije, H.H.G., Uhlenbrook, S., Kavetski, D., Pfister, L., 2015. Towards more systematic perceptual model development: a case study using 3 Luxembourgish catchments. Hydrol. Process. 29, 2731–2750. https://doi.org/10.1002/hyp.10393.